Wave-to-Wire Control of an Oscillating Water Column Wave Energy System Equipped with a Wells Turbine

Marco Rosati, Hafiz Ahsan Said and John V. Ringwood

***Abstract*—Wave energy is a significant source of renewable energy which is harnessed by wave energy converters (WECs). However, the high levelised cost of energy (LCoE) associated with wave energy projects hinders the commercial development of WECs. To minimise the LCoE, comprehensive control strategies, to maximise electric energy production, are essential. The oscillating water column (OWC) is one of the most promising WECs for harnessing wave power, especially due to its relative simplicity of operation. Due to the overbearing issue of turbine efficiency, the vast majority of OWC control strategies focus on a simplified control objective, namely turbine efficiency maximisation. However, it is important to note that rotational speed control impacts generator performance. Additionally, for Wells turbines, rotational speed control also affects the hydrodynamic performance, specifically the wave-to-pneumatic energy conversion process. Therefore, Wells turbine rotational speed should be ideally modulated to improve the overall wave-to-wire (W2W) efficiency of the OWC system, rather than just turbine efficiency. In this paper, a control strategy for maximising W2W efficiency of a fixed OWC WEC, equipped with a Wells turbine, is designed. The proposed control strategy comprises two parts: Firstly, a 'global' setpoint, which considers the entire OWC W2W model, is derived. Secondly, a Lyapunov-based nonlinear controller is designed to track the aforementioned setpoint. Results from numerical simulation show that, in comparison to the somewhat traditional turbine efficiency maximising control approach, the proposed W2W control strategy significantly improves W2W efficiency for the considered sea states.**

***Index Terms*—oscillating water column, nonlinear control, wave-to-wire, wave energy, Wells turbine.**

I. Introduction

In order to advance towards a carbon-free society, diversification of the renewable energy resources is essential [1]. To this end, wave energy is a significant and relatively untapped source of renewable energy [2], which can considerably contribute to the renewable energy mix.

This paper is based upon work supported by MaREI, the SFI Research Centre for Energy, Climate and Marine, under grant No. 12/RC/2302 P2

Marco Rosati is a member of COER (Centre for Ocean Energy Research), Maynooth University, Maynooth, Co. Kildare, Ireland (e-mail: marco.rosati.2021@mumail.ie).

Hafiz Ahsan Said is a member of COER (Centre for Ocean Energy Research), Maynooth University, Maynooth, Co. Kildare, Ireland (e-mail: hafiz.said.2020@mumail.ie).

John V. Ringwood is the director of COER (Centre for Ocean Energy Research), Maynooth University, Maynooth, Co. Kildare, Ireland (e-mail: john.ringwood@mu.ie).

Digital Object Identifier:
https://doi.org/10.36688/ewtec-2023-309

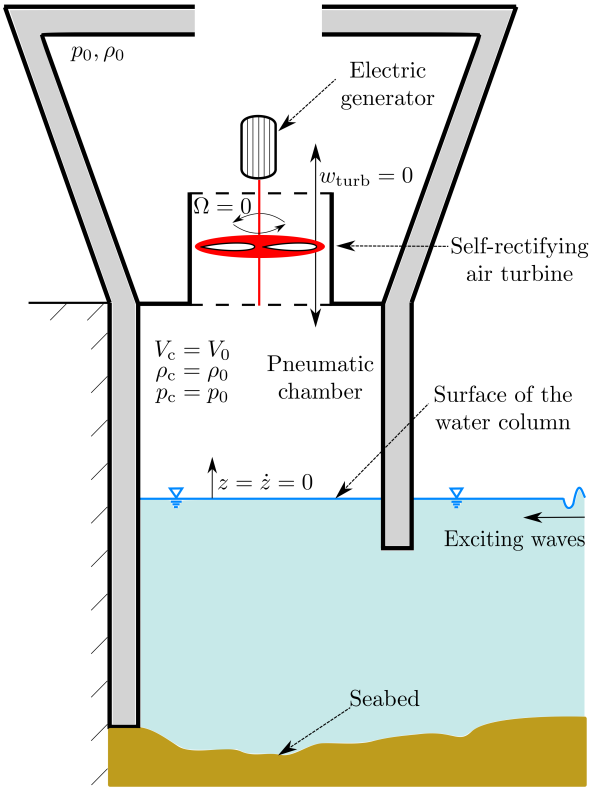

Fig. 1. Schematic of a fixed OWC WEC in still water conditions.

The oscillating water column (OWC) [3], schematically shown in Fig. 1, is one of the most promising types of wave energy converters (WECs) for harnessing wave power, especially due to its relatively simple operating principle and the fact that all the moving parts are above the water level. In essence, the OWC operating principle can be described as follows. The incoming ocean waves excite a water column which displaces (mainly) vertically. The water column displacement alternatively compresses/decompresses a volume of air in a pneumatic chamber and, consequently, a bidirectional air flow is generated. The inward/outward air flow is typically used to drive a self-rectifying air turbine [4]. Finally, the air turbine is directly coupled with a suitable electric generator [5], which converts the turbine mechanical power into electrical power.

To date, the commercial viability of WECs is thwarted by the relatively high levelised cost of energy (LCoE) characterising wave energy projects, defined as

$$\text{LCoE} = \frac{\text{CapEx} + \text{OpEx}}{\text{Produced energy over the WEC lifetime}}, \quad (1)$$

where CapEx and OpEx indicate the capital and operational costs, respectively. To minimise the LCoE, comprehensive control strategies to maximise electric energy production are vital [6], although produced energy maximisation does not necessarily improve WEC profitability (impact of control actions on costs also need to be considered).

Due to the important issue of turbine efficiency, the vast majority of OWC control strategies [7] focus on a *simplified* control objective, namely turbine efficiency maximisation [8]–[11]. While operating the air turbine around its maximum efficiency point (MEP) is a primary focus of OWC control strategies, it is important to note that rotational speed control also impacts generator performance. Additionally, for Wells turbines [4], rotational speed control also affects the OWC hydrodynamic performance [12], specifically the wave-to-pneumatic energy conversion process. Therefore, Wells turbine rotational speed should be ideally modulated to maximise the overall wave-to-wire (W2W) efficiency of the OWC system [13], rather than just turbine efficiency.

In this paper, a control strategy for maximising the W2W efficiency of a Mutriku-like [14] OWC WEC, equipped with a Wells turbine coupled with a permanent magnet synchronous generator (PMSG), is proposed. In general, the W2W WEC control problem can be tackled with an optimal control approach [15]–[17], or a somewhat more traditional control approach based on static efficiencies [18], [19]. For OWCs, the optimal control approach leads to a challenging online nonlinear constrained optimisation problem [15], [20], for which convexity is typically not guaranteed. In contrast to global optimisation methods, the W2W control strategy proposed in this paper is based on a relatively simple static efficiency approach, allowing for a straight comparison with the more traditional turbine efficiency maximising control approach. The proposed control strategy comprises two parts. Firstly, a 'global' setpoint, which considers the entire OWC W2W model (WEC hydrodynamics, Wells turbine, and generator dynamics), is derived. Secondly, a Lyapunov-based nonlinear controller [21] is designed to track the aforementioned setpoint. The results obtained from numerical simulation show that, in comparison to the somewhat traditional turbine efficiency maximising control approach, the proposed W2W control strategy leads to a significant improvement in the OWC W2W efficiency for the considered sea states. It is important to note that control co-design aspects should be considered to take full advantage of W2W control. To this end, in Section IV-C, the main control co-design aspects impacting W2W OWC control possibilities, such as the turbine efficiency characteristic and the type of air turbine, are highlighted.

The remaining structure of the paper is organised as follows. In Section II, a complete physics-based OWC W2W model is presented, with the proposed W2W OWC control strategy designed in Section III. In Section IV, the results of numerical simulation, as well as the main control co-design aspects, are discussed. Finally, some conclusive remarks can be found in Section V.

II. OWC Modelling

In this section, a complete physics-based W2W model for the fixed OWC WEC considered in this paper is provided. To simplify the notation, the time dependence of variables is omitted. A schematic of the W2W power train of the OWC WEC is depicted in Fig. 2.

A. Hydrodynamic modelling

Under the typical assumptions of linear potential theory, a hydrodynamic model for OWCs can be derived by modelling the water column as a neutrally buoyant piston [22]

$$m_{\mathrm{p}}\dot{v} = -\rho_{\mathrm{w}} g S_{\mathrm{w}} z - S_{\mathrm{w}} p_{\mathrm{c}} - f_{\mathrm{r}} + f_{\mathrm{ex}}, \tag{2}$$

where z is the position of the water column relative to the still water level, $v = \dot{z}$ is the velocity of the water column, m_{p} is the water piston mass, ρ_{w} is the water density, S_{w} is the OWC water plane area, g is the gravity acceleration constant, p_{c} is the air chamber pressure, f_{ex} indicates the excitation force due to an incident wave of frequency ω, and f_{r} is the force due to radiated waves. The excitation force at time t is computed as a sum of N frequency components, ω_{n}, as

$$f_{\mathrm{ex}} = \sum_{\mathrm{n}=1}^{N} A_{\mathrm{ex}}(\omega_{\mathrm{n}}) \cos(\omega_{\mathrm{n}}\, t + \phi_{\mathrm{ex}}(\omega_{\mathrm{n}})), \tag{3}$$

where ϕ_{ex} and A_{ex} are the phase and amplitude of the excitation force, respectively. Finally, the radiation force is written as

$$f_{\mathrm{r}} = A(\infty)\dot{v} + \int_{-\infty}^{t} k_{\mathrm{r}}(t-\tau)\, v(\tau)\, \mathrm{d}\tau, \tag{4}$$

where $A(\infty)$ is the OWC added mass at infinite frequency ($A(\omega)|_{\omega\to\infty} = A(\infty)$), while k_{r} is the piston impulse response function computed as the inverse Fourier transform of the OWC radiation damping, $B(\omega)$. To obtain the frequency dependant functions $A(\omega)$, $B(\omega)$, $A_{\mathrm{ex}}(\omega)$, and $\phi_{\mathrm{ex}}(\omega)$, a boundary element problem [23] is solved using the WAMIT software [24]. Following established practice in the wave energy field, a suitable (and less computationally expensive) linear state space model is adopted to approximate the convolution integral in Eq. (4). To this end, a Prony method is used [25].

B. Air chamber modelling

The air pressure evolution in the pneumatic chamber is modelled as

$$\frac{\dot{p}_{\mathrm{c}}}{p_{\mathrm{c}}} = -\frac{\gamma}{V_{\mathrm{c}}}\left(\dot{V}_{\mathrm{c}} + \frac{w_{\mathrm{turb}}}{\rho_{\mathrm{c}}}\right), \tag{5}$$

where γ is the air specific heat ratio, w_{turb} indicates the turbine air mass flow rate (positive for outward air flow), $V_{\mathrm{c}} = V_0 - S_{\mathrm{w}} z$ is the chamber air volume, V_0 is the air volume in still water conditions, and ρ_{c}

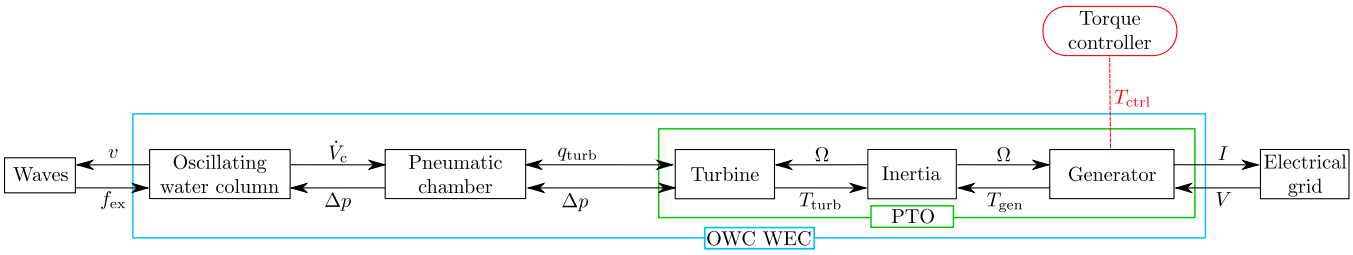

Fig. 2. Wave-to-wire power train of the OWC WEC considered in this paper. Adapted from [7].

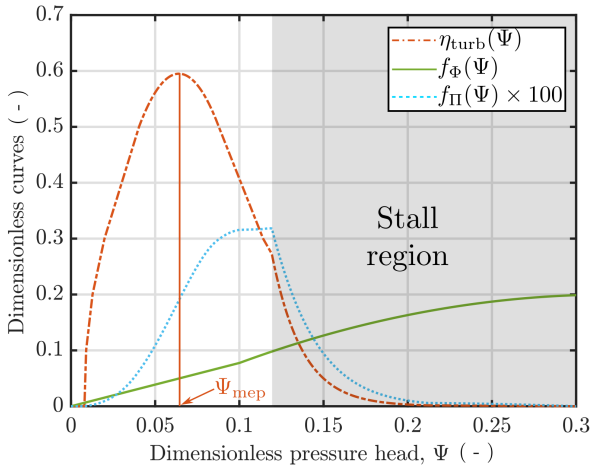

Fig. 3. Dimensionless flow rate, Φ, dimensionless power, Π, and turbine efficiency, η_{turb}, as functions of the dimensionless pressure head, Ψ, for the Wells turbine considered in this paper. The grey shaded area represents the turbine stall region.

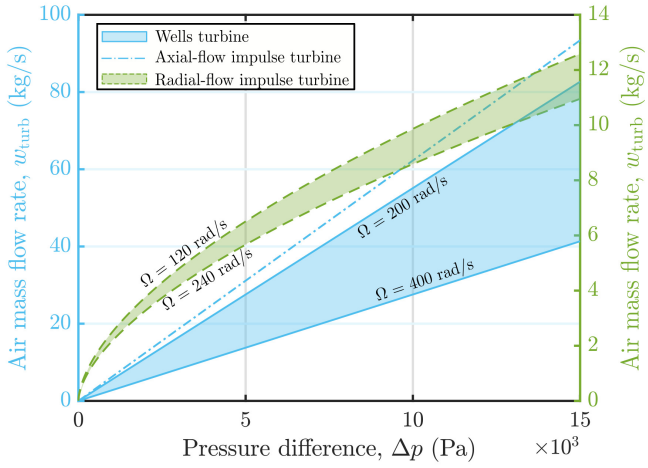

Fig. 4. Pressure difference vs mass flow rate for a Wells turbine with $d_{\text{r}} = 0.75$ m, and for two different types of impulse turbines, both with $d_{\text{r}} = 0.65$ m. The air density is considered constant, $\rho_{\text{air}} = \rho_0$.

is the air chamber density. For an isentropic compression/expansion process:

$$\rho_{\text{c}} = \rho_0 \left(\frac{p_{\text{c}}}{p_0}\right)^{1/\gamma}, \tag{6}$$

where the subscript '0' refers to standard atmosphere values for the corresponding thermodynamic variable.

C. Turbine/generator modelling

The dynamics of the turbine/generator set, if bearing friction losses are ignored, are modelled as

$$\frac{\text{d}}{\text{d}t}\left(\frac{1}{2} I \Omega^2\right) = P_{\text{turb}} - P_{\text{ctrl}}, \tag{7}$$

where Ω is the rotational speed of the turbine/generator set, I is the inertia moment of the rotating parts, P_{turb} is the turbine mechanical power, and $P_{\text{ctrl}} = T_{\text{ctrl}}\,\Omega$ is the generator control power, where T_{ctrl} is the generator control torque.

1) Air turbine modelling: If the Reynolds number is large ($\text{Re} > 10^6$) and Mach number is small ($\text{Ma} < 0.3$), the air turbine can be modelled using the following dimensionless functions [26]

$$\Phi = f_\Phi(\Psi),\ \Pi = f_\Pi(\Psi), \tag{8}$$

where Ψ is the dimensionless pressure head, Φ is the dimensionless air mass flow rate, and Π is the dimensionless turbine power. The dimensionless variables are defined as

$$\Phi = \frac{w_{\text{turb}}}{\rho_{\text{air}}\,\Omega\,d_{\text{r}}^3},\ \Pi = \frac{P_{\text{turb}}}{\rho_{\text{air}}\,\Omega^3\,d_{\text{r}}^5},\ \Psi = \frac{\Delta p}{\rho_{\text{air}}\,\Omega^2\,d_{\text{r}}^2}, \tag{9}$$

where d_{r} is the turbine rotor diameter, $\Delta p = p_{\text{c}} - p_0$ is the pressure difference between the chamber and the atmosphere, and $\rho_{\text{air}} = \max(\rho_{\text{c}}, \rho_0)$ is the air density. Finally, the turbine efficiency is defined as

$$\eta_{\text{turb}}(\Psi) = \frac{P_{\text{turb}}}{P_{\text{pneu}}} = \frac{f_\Pi(\Psi)}{\Psi\, f_\Phi(\Psi)}, \tag{10}$$

where $P_{\text{pneu}} = q_{\text{turb}}\,\Delta p$ is the pneumatic power available to the turbine and $q_{\text{turb}} = w_{\text{turb}}/\rho_{\text{air}}$ is the turbine volumetric flow rate. Figure 3 shows $f_\Phi(\Psi)$, $f_\Pi(\Psi)$, and $\eta_{\text{turb}}(\Psi)$ for the Wells turbine considered in this paper.

2) Turbine damping: For a Wells turbine, turbine damping depends on the rotational speed [4], as

$$\Theta = \frac{w_{\text{turb}}}{\Delta p} = \frac{d_{\text{r}}}{\kappa\,\Omega}, \tag{11}$$

meaning that Wells turbine rotational speed control impacts hydrodynamic performance. In Eq. (11), κ is a constant that depends on the turbine geometry. We note that, in contrast to the Wells turbine case, since impulse-like turbine damping only marginally depends on Ω [13], it is not possible to significantly affect the OWC hydrodynamic performance by modulating Ω. Fig. 4 shows the relationship between w_{turb} and Δp, as Ω varies, for different types of self-rectifying air turbines. Unsurprisingly, the Wells turbine has the greatest capability for influencing turbine damping, as indicated by the relatively large blue shaded area.

3) Generator modelling: The PMSG model in the direct/quadrature (denoted by the d/q subscripts) frame is specified [27] as

$$\begin{aligned}\frac{\mathrm{d}i_\mathrm{d}}{\mathrm{d}t} &= -\frac{R_\mathrm{d}}{L_\mathrm{d}}i_\mathrm{d} + \omega_\mathrm{e} i_\mathrm{q} + \frac{1}{L_\mathrm{d}}v_\mathrm{d} \\ \frac{\mathrm{d}i_\mathrm{q}}{\mathrm{d}t} &= -\frac{R_\mathrm{q}}{L_\mathrm{q}}i_\mathrm{q} - \omega_\mathrm{e} i_\mathrm{d} - \frac{\lambda\omega_\mathrm{e}}{L_\mathrm{q}} + \frac{1}{L_\mathrm{q}}v_\mathrm{q}\end{aligned} \tag{12}$$

and

$$T_\mathrm{ctrl} = \frac{3}{4}N_\mathrm{p}(i_\mathrm{q}\lambda - i_\mathrm{q}i_\mathrm{d}(L_\mathrm{d} - L_\mathrm{q})), \tag{13}$$

where $v_\mathrm{d}(v_\mathrm{q})$, $i_\mathrm{d}(i_\mathrm{q})$, $R_\mathrm{d}(R_\mathrm{q})$, and $L_\mathrm{d}(L_\mathrm{q})$ are, respectively, the stator voltage, the stator current, the stator resistance, and the stator inductance in the direct (quadrature) frame. Furthermore, $\omega_\mathrm{e} = (\Omega N_\mathrm{p})/2$, λ, and N_p are, respectively, the generator electric angular frequency, the rotor permanent magnet flux, and the number of poles. Finally, the generator active (real) power is written as

$$P_\mathrm{gen} = \frac{3}{2}(v_\mathrm{d}i_\mathrm{d} + v_\mathrm{q}i_\mathrm{q}) - \underbrace{(R_\mathrm{q}i_\mathrm{q}^2 + R_\mathrm{d}i_\mathrm{d}^2)}_{\text{copper losses}}. \tag{14}$$

It should be noted that, in this paper, since $R_\mathrm{d} = R_\mathrm{q} = R$ and $L_\mathrm{d} = L_\mathrm{q} = L$, Eqs. (12), (13), and (14) can be simplified.

III. W2W CONTROL DESIGN

This section describes the design procedure for the OWC W2W control approach proposed in this paper. A schematic of the W2W control structure can be found in Fig. 5.

A. Reference generation

To maximise the OWC W2W efficiency, the effect of Wells turbine rotational speed on the complete W2W system must be considered [19]. In this paper, eight irregular sea states (SS1 - SS8), generated from JONSWAP spectral density functions [28] with peak shape parameter $\gamma^J = 3.3$, are considered. The peak period, T_p, and significant wave height, H_s, of the eight sea states (reported in Tab. III-A) are selected considering the characteristic wave climate measured at the Mutriku power plant [14]. It should be noted that, to take into account the shoaling effect of the ocean waves at Mutriku, an attenuation function is used to modify the JONSWAP spectra, as detailed in [9].

The eight black curves in Fig. 6 represent the time-averaged electrical power, $\bar{P}_\mathrm{elec}$, as a function of Ω, for sea states SS1 - SS8. To compute the average electrical power, 20 distinct realizations with a time step of 0.005 s are run, for each sea state, and for different constant values of Ω, for 1200 s. A possible control strategy for maximising the OWC W2W efficiency is found by fitting a suitable function to the peak values of $\bar{P}_\mathrm{elec}$, as for the yellow power curve in Fig. 6. For the OWC system modelled in Section II, a W2W efficiency maximising power curve has the following form

$$P_\mathrm{ctrl}^\mathrm{w2w} = T_\mathrm{ctrl}^\mathrm{w2w}\,\Omega = \underbrace{l_1 + l_2\,\Omega}_{\text{linear term}} + \underbrace{e_1\,\exp^{e_2\,\Omega}}_{\text{exponential term}}, \tag{15}$$

TABLE I
PARAMETERS OF THE SEA STATES

Sea state	H_s (m)	T_p (s)
SS1	0.88	6.40
SS2	1.03	7.55
SS3	1.04	8.75
SS4	1.08	11.05
SS5	1.48	14.55
SS6	1.81	15.70
SS7	2.07	16.90
SS8	3.20	14.55

where $l_1 = 2.044 \times 10^{-8}$, $l_2 = 2.696$, $e_1 = 6.98$, and $e_2 = 0.02156$. When Ω is relatively low, the value of $P_\mathrm{ctrl}^\mathrm{w2w}$ in Eq. (15) is mainly driven by the linear term, whereas the exponential term dominates if Ω is high. From Eq. (15), the torque reference value for maximising W2W efficiency, $T_\mathrm{ctrl}^\mathrm{w2w}$, is derived as

$$T_\mathrm{ctrl}^\mathrm{w2w} = P_\mathrm{ctrl}^\mathrm{w2w}/\Omega = (l_1 + l_2\,\Omega\ + e_1\,\exp^{e_2\,\Omega})/\Omega, \tag{16}$$

To maximise turbine efficiency, a control law of the following form [8]

$$P_\mathrm{ctrl}^{\eta_\mathrm{turb}} = T_\mathrm{ctrl}^{\eta_\mathrm{turb}}\,\Omega = a_1\,\Omega^{a_2}, \tag{17}$$

can be used. To operate the turbine around its maximum efficiency point (see Ψ_mep in Fig. 3), the control parameters are set as $a_1 = \rho_\mathrm{air}\,d_\mathrm{r}^5\,f_\Pi(\Psi_\mathrm{mep})$ and $a_2 = 3$. Since $\rho_\mathrm{air} \approx \rho_0$, a_1 is approximately constant and, for the Wells turbine model of Fig. 3, $a_1 = 3 \times 10^{-4}$. To obtain the torque reference for turbine efficiency maximisation, $T_\mathrm{ctrl}^{\eta_\mathrm{turb}}$, Eq. (17) is rearranged as

$$T_\mathrm{ctrl}^{\eta_\mathrm{turb}} = P_\mathrm{ctrl}^{\eta_\mathrm{turb}}/\Omega = a_1\,\Omega^{a_2-1}. \tag{18}$$

It is important to note that, in contrast with the purely data-based W2W power curve in Eq. (15), the turbine efficiency maximising control torque in Eq. (18) is derived analytically [8]. Furthermore, the control law in Eq. (18) is not turbine-specific, therefore is valid for any type of turbine, while the control law in Eq. (16) is specific for the OWC W2W system modelled in Section II.

Finally, the electric current reference values are designed as follows. The value of $i_\mathrm{d}^\mathrm{ref}$ is set to zero to minimise generator copper losses (Cu-losses), while $i_\mathrm{q}^\mathrm{ref}$ is derived from Eq. (13), as

$$i_\mathrm{q}^\mathrm{ref} = \frac{4}{3}\frac{T_\mathrm{ctrl}^\mathrm{ref}}{N_\mathrm{p}\lambda}. \tag{19}$$

In Eq. (19), if $T_\mathrm{ctrl}^\mathrm{ref} = T_\mathrm{ctrl}^\mathrm{w2w}$ (see Eq. (16)), W2W efficiency is maximised, whereas if $T_\mathrm{ctrl}^\mathrm{ref} = T_\mathrm{ctrl}^{\eta_\mathrm{turb}}$ (see Eq. (18)), turbine efficiency is maximised.

B. Lyapunov-based torque controller

For tracking $i_\mathrm{d}^\mathrm{ref}$ and $i_\mathrm{q}^\mathrm{ref}$, a Lyapunov-based nonlinear controller is selected. The choice of a nonlinear controller is naturally motivated by the fact that the OWC W2W system dynamic is nonlinear. Furthermore, WECs operate in different irregular sea states, for

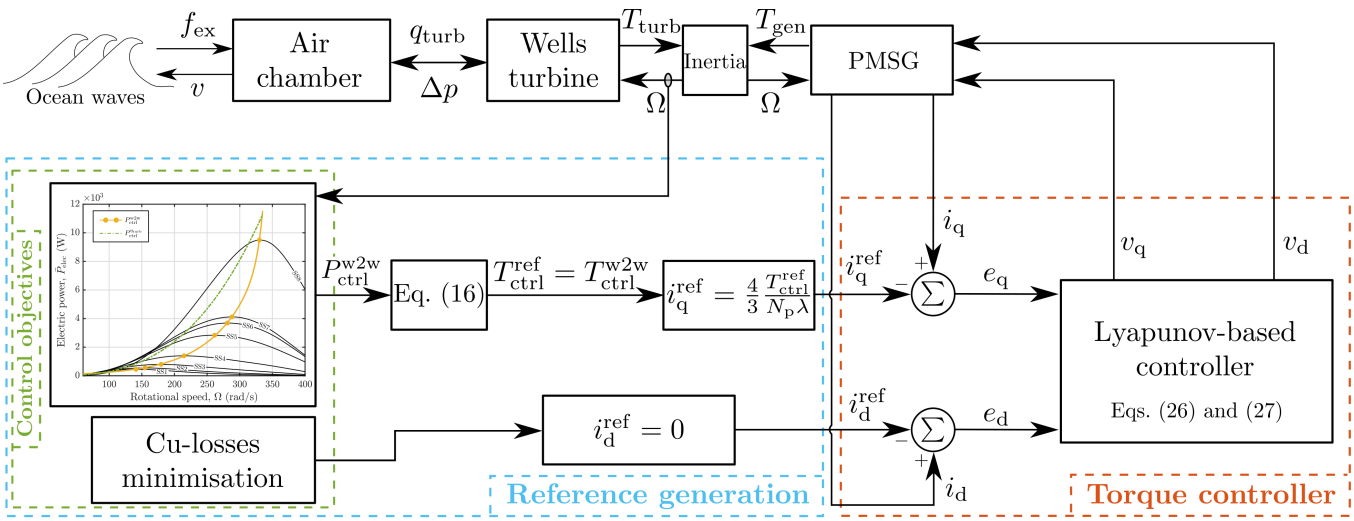

Fig. 5. Control structure for W2W efficiency maximisation with reference generation and torque controller. For turbine efficiency maximisation, the same control structure is used but P_{ctrl}^{w2w} becomes $P_{ctrl}^{\eta_{turb}}$, while Eq. (16) is replaced with Eq. (18) (i.e., $T_{ctrl}^{ref} = T_{ctrl}^{\eta_{turb}}$).

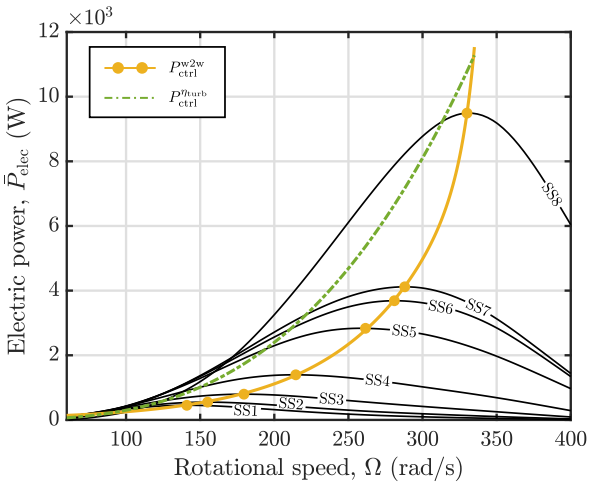

Fig. 6. The black curves represent $\bar{P}_{elec}$ as a function of Ω for different sea states. The two control curves P_{ctrl}^{w2w}, from Eq. (15), and $P_{ctrl}^{\eta_{turb}}$, from Eq. (17), are also shown.

which the relatively limited control envelop characterising typical linear controllers (e.g., PID controllers) may not suffice [29]. To cope with multiple irregular sea states, some solutions that use linear controllers with adaptive gains have emerged [10], [11]. However, these adaptive linear controllers generally require the solution of an optimisation problem in real-time to solve for the control gains, with an associated increase in the computational burden. In any case, the ability of linear controllers to handle the intrinsic nonlinear dynamics of the OWC remains questionable [7]. Among all the possible nonlinear controllers, Lyapunov-based stabilising control is computationally efficient and ensures the stability of the nonlinear system using the Lyapunov stability criterion [30].

To design the Lyapunov-based controller, the following tracking error signals are introduced

$$e_q = i_q - i_q^{ref}, \tag{20}$$

$$e_d = i_d - i_d^{ref}. \tag{21}$$

The desired control objectives (W2W/turbine efficiency maximisation and Cu-loss minimisation) are achieved if e_q and e_d are driven to zero, in a finite time interval. To this end, the dynamics of e_q and e_d, specified as

$$\dot{e}_q = -\frac{R_q}{L_q} i_q - \omega_e i_d - \frac{\lambda \omega_e}{L_q} + \frac{1}{L_q} v_q - \dot{i}_q^{ref} \tag{22}$$

and

$$\dot{e}_d = -\frac{R_d}{L_d} i_d + \omega_e i_q + \frac{1}{L_d} v_d - \dot{i}_d^{ref}, \tag{23}$$

are derived using Eq. (12). To force e_q and e_d to zero, $\dot{e}_q$ and $\dot{e}_d$ are designed, respectively, as

$$\dot{e}_q = -c_q e_q \tag{24}$$

$$\dot{e}_d = -c_d e_d, \tag{25}$$

where $c_q > 0$ and $c_d > 0$ are user defined control parameters. In this paper, the control parameters are set as $c_q = 120$ and $c_d = 90$. Finally, combining Eqs. (22)-(25), the (electric) control inputs v_q and v_d are derived, respectively, as

$$v_q = R_q i_q + (L_q i_d + \lambda)\omega_e + L_q(\dot{i}_q^{ref} - c_q e_q), \tag{26}$$

$$v_d = R_d i_d - L_d \omega_e i_q + L_d(\dot{i}_d^{ref} - c_d e_d). \tag{27}$$

The Lyapunov stability analysis for the control system can be found in Appendix A.

IV. Results and Discussion

The results of the numerical simulation are reported in Section IV-A and discussed in Section IV-B. Finally, some key control co-design aspects are considered in Section IV-C. The values of the OWC system parameters used in the numerical simulation are detailed in Tab. II.

A. Results of the numerical simulation

The W2W efficiency maximising, and turbine efficiency maximising, control strategies are tested in numerical simulation, where Lyapunov-based controllers are used for tracking $i_{\mathrm{q}}^{\mathrm{ref}}$ and $i_{\mathrm{d}}^{\mathrm{ref}}$. For each control strategy, and for all the considered sea state conditions (SS1-SS8), numerical simulations with a time step of 0.005 s are run for 1200 s.

By way of example, Figure 7 shows the time series of P_{pneu}, P_{turb}, P_{gen}, and η_{turb}, for a realization of SS4, when using the W2W efficiency maximising control approach. For each subplot, the horizontal dashed orange lines represent the respective time-averaged values.

Table IV-A reports the mean percentage values of the quantities of interest obtained from 20 distinct sea state realizations. In particular, for each realization, the time-averaged turbine efficiency, $\bar{\eta}_{\mathrm{turb}}$, the hydrodynamic capture width ratio (CWR), ξ_{hydro}, and the electric CWR, ξ_{elec}, defined as

$$\xi_{\mathrm{hydro}} = \frac{\bar{P}_{\mathrm{pneu}}}{\bar{P}_{\mathrm{wave}}\, l}, \; \xi_{\mathrm{elec}} = \frac{\bar{P}_{\mathrm{gen}}}{\bar{P}_{\mathrm{wave}}\, l} \tag{28}$$

are computed. In Eq. (28), $\bar{P}_{\mathrm{pneu}}$ is the time-averaged pneumatic power, $\bar{P}_{\mathrm{gen}}$ is the time-averaged generator electric power, $\bar{P}_{\mathrm{wave}}$, which is a function of the sea state, is the time-averaged wave power per metre of wave crest, and l is the OWC capture width. It should be noted that ξ_{hydro} is the wave-to-pneumatic efficiency (or hydrodynamic efficiency), whereas ξ_{elec} is essentially the OWC W2W efficiency. Finally, Tab. IV-A also reports the relative increase in the time-averaged generator electrical power, $\bar{P}_{\mathrm{gen}}^{\%}$, obtained using the different control torques in Eqs. (16) and (18).

B. Discussion

In comparison to the turbine efficiency maximising strategy, the W2W efficiency maximising control approach leads to higher values of ξ_{elec}, for all the considered sea states (see Tab. IV-A). Indeed, although $\bar{\eta}_{\mathrm{turb}}$ is slightly penalised when $T_{\mathrm{ctrl}}^{\mathrm{w2w}}$ is used, the overall W2W performance of the OWC system significantly improves, especially for medium-to-high energy sea states (SS4 - SS8). In particular, from Tab. IV-A, it is possible to note that ξ_{hydro} is always superior with Eq. (16) rather than with Eq. (18), meaning that the W2W control approach better accounts for the impact of Ω on the OWC hydrodynamic efficiency. It should be also noted that, since T_{p} in SS4 is close to one of resonance conditions of the Mutriku plant [9], ξ_{elec} and ξ_{hydro} are relatively high in SS4, providing that Ω is appropriately controlled [19].

In relation to current reference tracking performance,

TABLE II
OWC SYSTEM PARAMETERS

Parameter	Value	Unit	Parameter	Value	Unit
m_{p}	27748	kg	I	3.06	kg m^2
$A(\infty)$	71618	kg	κ	0.775	-
l	4.5	m	λ	0.92	Wb
d_{r}	0.75	m	N_{p}	4	-
S_{w}	19.35	m^2	R	0.08	ohm
V_0	144	m^3	L	0.003	H

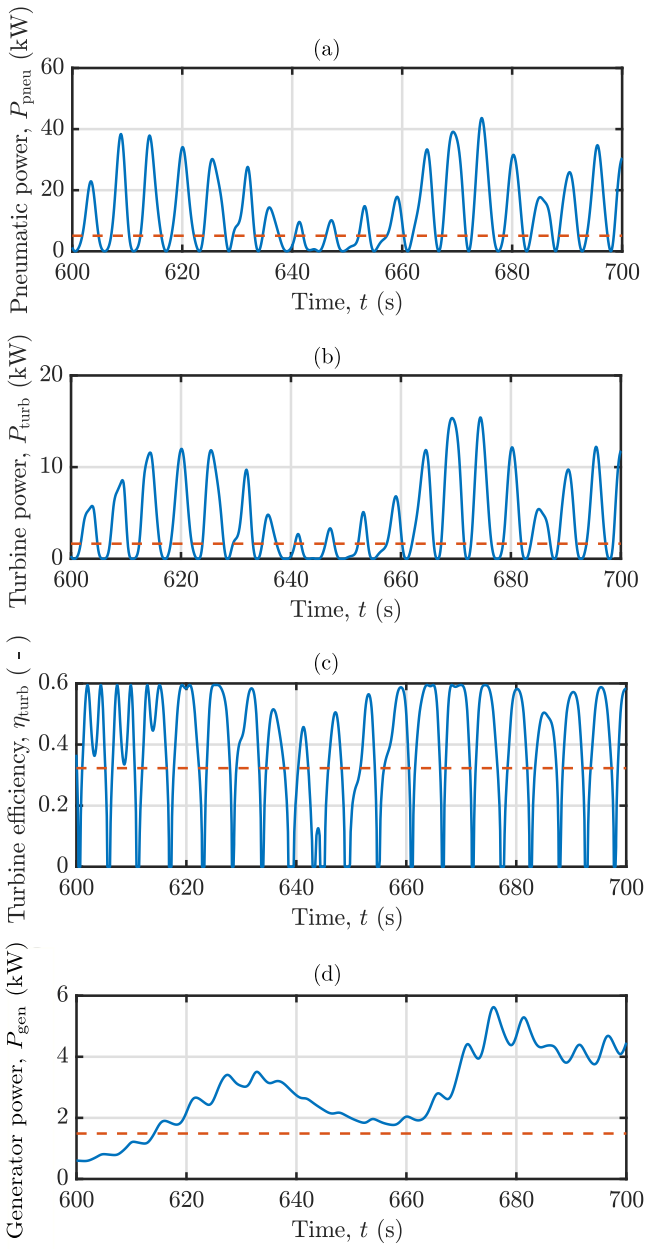

Fig. 7. Time series of P_{pneu}, P_{turb}, P_{gen}, and η_{turb}, for SS4, using $T_{\mathrm{ctrl}}^{\mathrm{w2w}}$ in Eq. (16). The dashed orange lines represent the corresponding time averaged values.

TABLE III
RESULTS OF THE SIMULATIONS

SS	Eq. (16): $T_{\mathrm{ctrl}}^{\mathrm{w2w}}$			Eq. (18): $T_{\mathrm{ctrl}}^{\eta_{\mathrm{turb}}}$			$\bar{P}_{\mathrm{gen}}^{\%}$
	$\bar{\eta}_{\mathrm{turb}}$	ξ_{elec}	ξ_{hydro}	$\bar{\eta}_{\mathrm{turb}}$	ξ_{elec}	ξ_{hydro}	
SS1	32.4	10.0	34.5	37.1	9.1	33.2	~ 0
SS2	32.5	9.7	34.0	36.8	8.9	33.0	~ 0
SS3	32.2	11.6	41.7	36.7	9.8	38.6	1.3
SS4	33.2	15.0	53.9	37.8	12.3	46.0	2.4
SS5	35.2	14.8	48.5	37.5	9.9	38.9	11.3
SS6	35.3	12.7	42.5	38.4	11.6	41.5	3.2
SS7	34.9	10.0	34.8	38.6	8.3	30.1	6.4
SS8	38.7	13.0	52.0	39.3	11.4	45.2	14.3

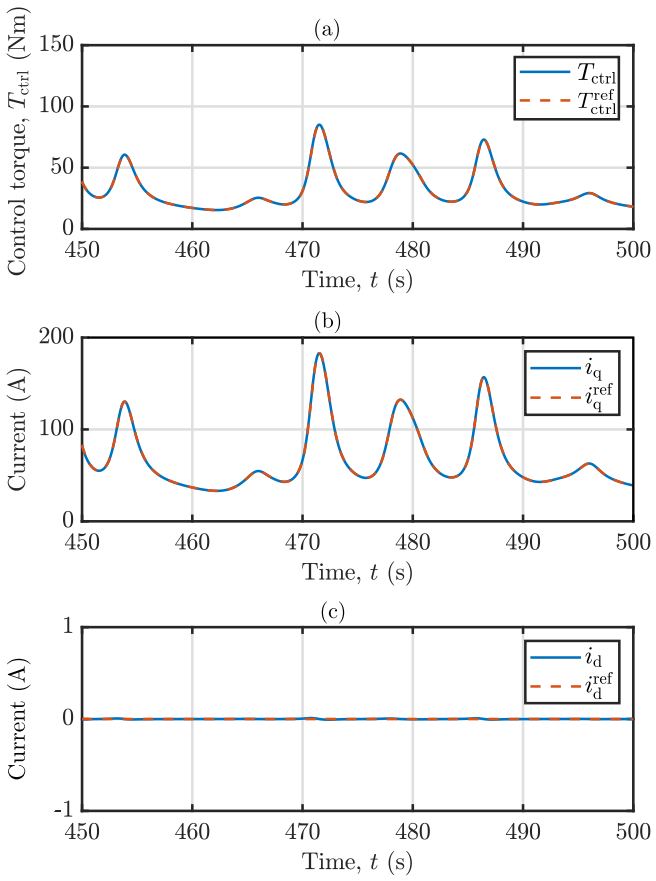

Fig. 8. Tracking performance for (a) $T_{\rm ctrl}$, (b) $i_{\rm q}$, and (c) $i_{\rm d}$ using W2W efficiency maximising control in SS8.

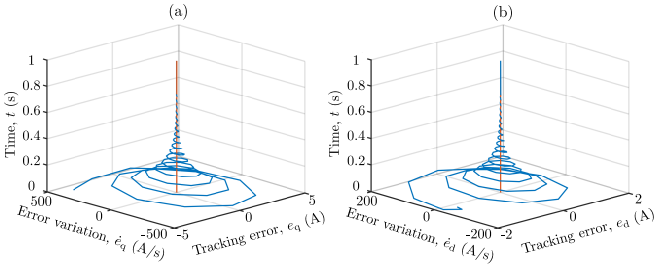

Fig. 9. Trajectories of (a) $e_{\rm q}/\dot{e}_{\rm q}$ and (b) $e_{\rm d}/\dot{e}_{\rm d}$ using W2W efficiency maximising control in SS8.

the Lyapunov-based nonlinear controller is able to properly track $i_{\rm d}^{\rm ref}$ and $i_{\rm q}^{\rm ref}$ (and, consequently, $T_{\rm ctrl}^{\rm ref}$), even in the relatively high energy sea states. For instance, Fig. 8 shows the tracking performance for $T_{\rm ctrl}$, $i_{\rm q}$, and $i_{\rm d}$ in SS8, sea state for which the root-mean-squared values of the tracking errors are the highest. For 20 realisations of SS8, using the W2W control strategy, the average root-mean-square values of the tracking errors $e_{\rm q}$, $e_{\rm d}$, and $e_{\rm ctrl} = T_{\rm ctrl} - T_{\rm ctrl}^{\rm ref}$ are, respectively, 0.26 A, 0.35 A, and 0.12 Nm. Furthermore, Fig. 9 shows the trajectories of $e_{\rm q}$ ($\dot{e}_{\rm q}$) and $e_{\rm d}$ ($\dot{e}_{\rm d}$) during the first second of a realisation of SS8. It can be noted that the errors, and the corresponding time derivatives, are driven to zero in about 0.8 s.

C. Main control co-design aspects

WEC geometry optimisation is significantly influenced by control-related aspects and, therefore, WEC control strategies should be considered from an early stage of the WEC design [31]. In particular, since Wells turbine rotational speed modulation affects all the energy conversion processes of an OWC system, it is crucial to adopt control co-design techniques for maximising the benefit of W2W control.

Firstly, as already mentioned, the W2W control strategy designed in this paper is effective only with a Wells turbine. Indeed, rotational speed control for impulse-like turbines does not significantly impact hydrodynamic performance. For instance, Fig. 10 shows how $\bar{\eta}_{\rm turb}$ and $\xi_{\rm hydro}$ vary for fifteen evenly spaced constant values of the rotational speed (from 50 rad/s to 400 rad/s), for two different turbine types, in SS4. For each turbine type, the rectangular shaded area represents the range of possible values of $\xi_{\rm hydro}$. As expected, with a radial-flow impulse turbine (the model for which is available in [13]), rotational speed control primarily influences $\bar{\eta}_{\rm turb}$, while $\xi_{\rm hydro}$ is only moderately affected by Ω. Therefore, rotational speed control for radial-flow impulse turbines should prioritize turbine efficiency maximisation, as a control objective. For the Wells turbine, $\xi_{\rm hydro}$ varies from 0.19 (for $\Omega = 50$ rad/s) to 0.63 (for $\Omega = 400$ rad/s), meaning that a somewhat more careful modulation of Ω is required to take into account the effect of the hydrodynamic/aerodynamic interaction.

In relation to W2W performance in SS4, the green dotted circles in Fig. 10 indicate the case in which the best trade-off between $\bar{\eta}_{\rm turb}$ and $\xi_{\rm hydro}$ is achieved (or, equivalently, the aerodynamic CWR, $\xi_{\rm aero} = \xi_{\rm hydro}\,\bar{\eta}_{\rm turb}$, is maximum), while the yellow circles highlight the condition in which $\xi_{\rm elec}$ is maximised. For the Wells turbine, the maximum values of $\bar{\eta}_{\rm turb}$, $\xi_{\rm hydro}$, $\xi_{\rm aero}$, and $\xi_{\rm elec}$ are found for four distinct operating conditions. With a radial-flow impulse turbine, when $\bar{\eta}_{\rm turb}$ is maximum, $\xi_{\rm elec}$ and $\xi_{\rm aero}$ are also maximised, meaning that rotational speed control is, to some extent, simpler.

Regarding the Wells turbine efficiency curve, to enhance the control envelope (possibility) for Ω, a Wells turbine with a relatively flat efficiency curve should be designed/selected. In fact, if a Wells turbine with a high-valued and flat efficiency curve is available, Ω can be modulated to improve hydrodynamic (and, to a lesser extent, generator) performance more freely. On the other hand, a peaky turbine efficiency curve intrinsically limits the control possibility for Ω and, in this case, rotational speed control should focus on turbine efficiency maximisation.

In addition to the overbearing issue of turbine efficiency, which is characterised by a limited high efficiency region (see Fig. 3), a minor issue concerns the impact of Ω on the electric generator efficiency. Providing that a suitable generator is selected [5], the generator efficiency is relatively high in the typical range of Ω experienced by the OWC PTO mechanism. In particular, among all possible electric generators for OWC WECs, PMSGs have a relatively large operating range in terms of Ω [32], meaning that PMSG performance is only marginally sensitive to rotational speed control. On the downside, due to the need for per-

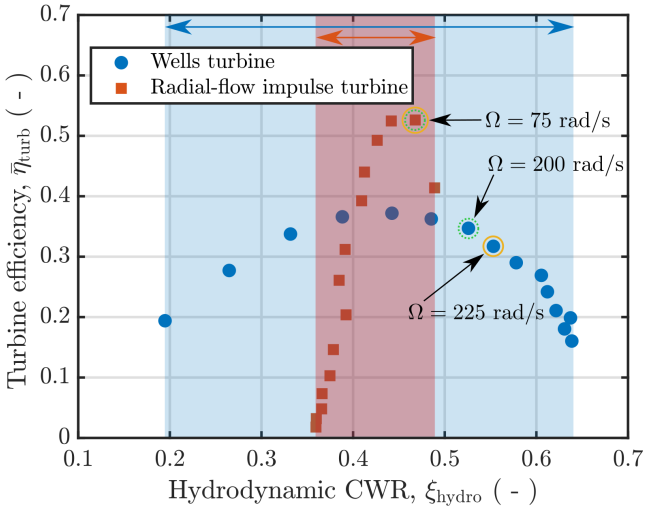

Fig. 10. ξ_{hydro} and $\bar{\eta}_{\text{turb}}$ for fifteen constant values of Ω, in SS4. For each turbine type, the corresponding shaded area represents the range of possible values of ξ_{hydro}.

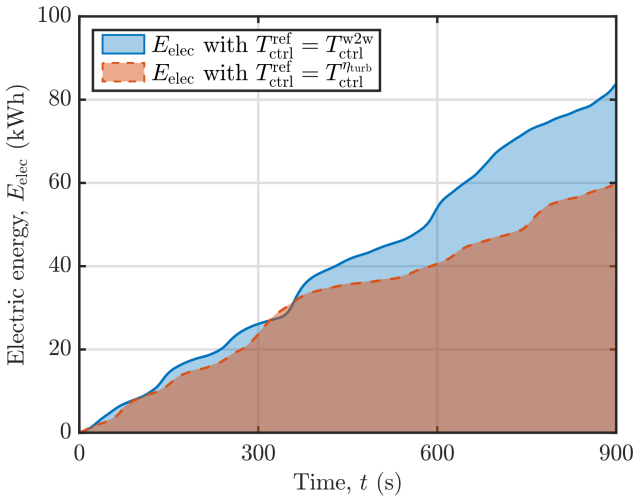

Fig. 11. Produced electric energy, E_{elec}, using turbine efficiency maximising control ($T^{\text{ref}}_{\text{ctrl}} = T^{\eta_{\text{turb}}}_{\text{ctrl}}$) and W2W efficiency maximising control ($T^{\text{ref}}_{\text{ctrl}} = T^{\text{w2w}}_{\text{ctrl}}$), in SS4.

manent magnets, PMSGs are typically more expensive then other possible electric generators for OWCs [5]. However, since PMSGs are brushless generators, and therefore require less frequent maintenance [32], OpEx is potentially lower.

V. Conclusion

In this paper, a W2W efficiency maximising control approach, based on steady-state efficiency is proposed for a fixed OWC equipped with a Wells turbine. In light of the discussion in Section IV-B, electric energy production significantly improves (see, for instance, Fig. 11) if the Wells turbine rotational speed is controlled considering the complete W2W OWC system. To take full advantage of the W2W control approach described in Section III, it is imperative to consider control co-design aspects (see Section IV-C). Furthermore, for the OWC system considered in this paper, the Lyapunov-based controller designed in Section III-B is able to provide suitable tracking performance (see Figs. 8 and 9).

Apart from the relative simplicity and low computational cost, the control approach proposed in this paper has a further advantage over a global online optimisation approach. In particular, model-based WEC control strategies may be sensitive to specific WEC modelling errors [33]. It should be noted that the static efficiency method is oblivious to some model uncertainties, specifically uncertainties related to the setpoint determination. In contrast, global online optimisation approaches include all model uncertainties, which may potentially compromise control performance. Furthermore, since real-time control is more difficult with a global online optimisation approach, free surface elevation [34] or pressure forecasting [35] may also be required to optimise the control action.

Finally, it should be mentioned that power dissipation control [13], power quality issues and grid-side control aspects [36], and the 'quantitative' impact of the control action on OpEx [37] are not considered in this paper. In comparison to a control approach based on static (steady-state) efficiencies, if power dissipation control is considered, a global optimisation approach may better take into account the interaction between peak-shaving and W2W efficiency maximising control.

Appendix A
Stability Analysis

The stability of the control system is assessed using Lyapunov stability criteria [30] and, to this end, a candidate Lyapunov function, $V(\mathbf{e}) : \mathbb{R}^2 \to \mathbb{R}_{\geq 0}$, with $\mathbf{e} = [e_{\text{q}}\ e_{\text{d}}]^T \in \mathbb{R}^{2\times 1}$, is introduced. If $V(\mathbf{e})$ has the following properties:

$$\begin{aligned} &(1)\, V(\mathbf{e}) > 0,\ \forall\, \mathbf{e} \neq \mathbf{0};\\ &(2)\, V(\mathbf{0}) = 0;\\ &(3)\, V(\mathbf{e}) = 0,\ \text{if}\ ||\mathbf{e}|| = 0;\\ &(4)\, \dot{V}(\mathbf{e}) < 0,\ \forall\, \mathbf{e} \neq \mathbf{0}; \end{aligned} \tag{29}$$

the system is asymptotically stable. A quadratic function in $\mathbf{e}$, specified as $V(\mathbf{e}) = \frac{1}{2}\mathbf{e}^T Q\, \mathbf{e}$ (with $Q \in \mathbb{R}^{2\times 2}$ symmetric and positive definite), is typically chosen as a candidate Lyapunov function. In particular, we consider a quadratic energy Lyapunov function of the following form

$$V(\mathbf{e}) = \frac{1}{2}[e_{\text{q}}\ e_{\text{d}}] \begin{bmatrix} L_{\text{q}} & 0 \\ 0 & L_{\text{d}} \end{bmatrix} \begin{bmatrix} e_{\text{q}} \\ e_{\text{d}} \end{bmatrix} = \frac{1}{2}(L_{\text{q}} e_{\text{q}}^2 + L_{\text{d}} e_{\text{d}}^2), \tag{30}$$

and, since $L_{\text{q}} = L_{\text{d}} = L$, Eq. (30) is simplified as

$$V(\mathbf{e}) = \frac{1}{2} L (e_{\text{q}}^2 + e_{\text{d}}^2). \tag{31}$$

The quadratic energy Lyapunov function in Eq. (31) directly satisfies the properties (1), (2), and (3) in Eq. (29). The time derivative of Eq. (31) leads to

$$\dot{V}(\mathbf{e}) = L(e_{\text{q}} \dot{e}_{\text{q}} + e_{\text{d}} \dot{e}_{\text{d}}). \tag{32}$$

To satisfy the fourth property in Eq. (29), $\dot{e}_{\text{q}}$ and $\dot{e}_{\text{d}}$ are designed, respectively, as specified in Eqs. (24) and (25):

$$\dot{V}(\mathbf{e}) = -L(c_{\text{q}}\, e_{\text{q}}^2 + c_{\text{d}}\, e_{\text{d}}^2). \tag{33}$$

Since c_{q}, $c_{\mathrm{d}} \in \mathbb{R}_{>0}$, it is straightforward to see that $\dot{V}(\mathbf{e}) < 0 \, \forall \, \mathbf{e} \neq \mathbf{0}$, which complete the proof.

REFERENCES

[1] X. Li, "Diversification and localization of energy systems for sustainable development and energy security," *Energy Policy*, vol. 33, no. 17, pp. 2237–2243, 2005.

[2] S. Astariz and G. Iglesias, "The economics of wave energy: A review," *Renewable and Sustainable Energy Reviews*, vol. 45, pp. 397–408, 2015.

[3] A. F. Falcão and J. C. Henriques, "Oscillating-water-column wave energy converters and air turbines: A review," *Renewable Energy*, vol. 85, pp. 1391–1424, 2016.

[4] A. F. O. Falcão and L. M. C. Gato, "Air turbines," in *Comprehensive Renewable Energy*, A. Sayigh, Ed. Oxford: Elsevier, 2012, vol. 8, pp. 111–149.

[5] D. L. O'Sullivan and A. W. Lewis, "Generator selection and comparative performance in offshore oscillating water column ocean wave energy converters," *IEEE Transaction on Energy Conversion*, vol. 26, no. 2, pp. 603–614, 2011.

[6] G. Chang, C. A. Jones, J. D. Roberts, and V. S. Neary, "A comprehensive evaluation of factors affecting the levelized cost of wave energy conversion projects," *Renewable Energy*, vol. 127, pp. 344–354, 2018.

[7] M. Rosati, J. C. C. Henriques, and J. V. Ringwood, "Oscillating-water-column wave energy converters: A critical review of numerical modelling and control," *Energy Conversion and Management X*, vol. 16, p. 100322, 2022.

[8] P. A. P. Justino and A. F. O. Falcão, "Rotational Speed Control of an OWC Wave Power Plant," *Journal of Offshore Mechanics and Arctic Engineering*, vol. 121, no. 2, pp. 65–70, 05 1999.

[9] J. C. C. Henriques, J. C. C. Portillo, W. Sheng, L. M. C. Gato, and A. F. O. Falcão, "Dynamics and control of air turbines in oscillating-water-column wave energy converters: Analyses and case study," *Renewable and Sustainable Energy Reviews*, vol. 112, pp. 571–589, 2019.

[10] K. Ezhilsabareesh, R. Suchithra, and A. Samad, "Performance enhancement of an impulse turbine for OWC using grouped grey wolf optimizer based controller," *Ocean Engineering*, vol. 190, p. 106425, 2019.

[11] F. M'zoughi, S. Bouallègue, A. J. Garrido, I. Garrido, and M. Ayadi, "Fuzzy gain scheduled pi-based airflow control of an oscillating water column in wave power generation plants," *IEEE Journal of Oceanic Engineering*, vol. 44, no. 4, pp. 1058–1076, 2019.

[12] M. Rosati and J. V. Ringwood, "Towards hydrodynamic control of an oscillating water column wave energy converter," *Trends in Renewable Energy Offshore*, pp. 411–418, 2022.

[13] M. Rosati, J. V. Ringwood, and J. C. C. Henriques, "A comprehensive wave-to-wire control formulation for oscillating water column wave energy converters," *Trends in Renewable Energy Offshore*, pp. 329–337, 2022.

[14] Y. Torre-Enciso, I. Ortubia, L. I. L. De Aguileta, and J. Marqués, "Mutriku wave power plant: From the thinking out to the reality," in *Proc. of the 8th European Wave and Tidal Energy Conference*, Uppsala, Sweden, 2009, pp. 319–329.

[15] J. M. Silva, S. M. Vieira, D. Valério, and J. C. C. Henriques, "GA-optimized inverse fuzzy model control of OWC wave power plants," *Renewable Energy*, vol. 8, pp. 17–29, 2023.

[16] N. Y. Sergiienko, G. Bacelli, R. G. Coe, and B. S. Cazzolato, "A comparison of efficiency-aware model-predictive control approaches for wave energy devices," *Journal of Ocean Engineering and Marine Energy*, vol. 8, no. 1, pp. 17–29, 2022.

[17] A. S. Haider, T. K. Brekken, and A. McCall, "Application of real-time nonlinear model predictive control for wave energy conversion," *IET Renewable Power Generation*, vol. 15, no. 14, pp. 3331–3340, 2021.

[18] D. García-Violini, N. Faedo, F. Jaramillo-Lopez, and J. V. Ringwood, "Simple controllers for wave energy devices compared," *Journal of Marine Science and Engineering*, vol. 8, no. 10, p. 793, 2020.

[19] M. Rosati and J. V. Ringwood, "Wave-to-wire efficiency maximisation for oscillating water column systems," in *Proceedings of the 22nd IFAC World Congress*. Yokohama, Japan: International Federation of Automatic Control, 2023.

[20] M. E. Magaña, C. Parlapanis, D. T. Gaebele, and O. Sawodny, "Maximization of wave energy conversion into electricity using oscillating water columns and nonlinear model predictive control," *IEEE Transaction on Sustainable Energy*, vol. 13, no. 3, pp. 1283–1292, 2022.

[21] W. E. Dixon, A. Behal, D. M. Dawson, and S. P. Nagarkatti, *Nonlinear control of engineering systems: A Lyapunov-based approach*. Springer Science & Business Media, 2003.

[22] D. V. Evans, "The oscillating water column wave-energy device," *IMA Journal of Applied Mathematics*, vol. 22, no. 4, pp. 423–433, 1978.

[23] J. Falnes, *Wave Interaction with Oscillating Water Columns*. Cambridge University Press, 2002, p. 225–262.

[24] J. N. Ewman and C. H. Lee, "WAMIT user manual," 2016, last accessed 02 March 2019. [Online]. Available: http://www.wamit.com/manual.htm

[25] W. Sheng, R. Alcorn, and A. Lewis, "A new method for radiation forces for floating platforms in waves," *Ocean Engineering*, vol. 105, pp. 43–53, 2015.

[26] S. L. Dixon and C. Hall, *Fluid mechanics and thermodynamics of turbomachinery*. Butterworth-Heinemann, 2013.

[27] N. Mohan, *Advanced Electric Drives: Analysis, Control, and Modeling Using MATLAB/Simulink*. Hoboken, USA: John Wiley & Sons, Ltd, 2014, ch. 10, pp. 143–156.

[28] K. Hasselmann *et al.*, "Measurements of wind-wave growth and swell decay during the joint north sea wave project (JONSWAP)." *Deutches Hydrographisches Institut*, 1973.

[29] A. J. Garrido, I. Garrido, M. Amundarain, M. Alberdi, and M. De la Sen, "Sliding-mode control of wave power generation plants," *IEEE Transaction on Industrial Applications*, vol. 48, no. 6, pp. 2372–2381, 2012.

[30] M. Kabalan, P. Singh, and D. Niebur, "Large signal lyapunov-based stability studies in microgrids: A review," *IEEE Transactions on Smart Grid*, vol. 8, no. 5, pp. 2287–2295, 2016.

[31] P. B. Garcia-Rosa, G. Bacelli, and J. V. Ringwood, "Control-informed geometric optimization of wave energy converters: The impact of device motion and force constraints," *Energies*, vol. 8, no. 12, pp. 13 672–13 687, 2015.

[32] S. Benelghali, M. Benbouzid, and J. Charpentier, "Comparison of PMSG and DFIG for marine current turbine applications," in *The XIX International Conference on Electrical Machines - ICEM 2010*, Rome, Italy, 2010, pp. 1–6.

[33] J. V. Ringwood, A. Mérigaud, N. Faedo, and F. Fusco, "An analytical and numerical sensitivity and robustness analysis of wave energy control systems," *IEEE Transactions on Control Systems Technology*, vol. 28, no. 4, pp. 1337–1348, 2020.

[34] F. Paparella, K. Monk, V. Winands, M. F. P. Lopes, D. Conley, and J. V. Ringwood, "Up-wave and autoregressive methods for short-term wave forecasting for an oscillating water column," *IEEE Transaction on Sustainable Energy*, vol. 6, no. 1, pp. 171–178, 2015.

[35] J. Marques Silva, S. M. Vieira, D. Valério, J. C. C. Henriques, and P. D. Sclavounos, "Air pressure forecasting for the mutriku oscillating-water-column wave power plant: Review and case study," *IET Renewable Power Generation*, vol. 15, no. 14, pp. 3485–3503, 2021.

[36] H. A. Said and J. V. Ringwood, "Grid integration aspects of wave energy—overview and perspectives," *IET Renewable Power Generation*, vol. 15, no. 14, pp. 3045–3064, 2021.

[37] K. M. Nielsen, T. S. Pedersen, P. Andersen, and S. Ambühl, "Optimizing Control of Wave Energy Converter with Losses and Fatigue in Power Take off," *IFAC-PapersOnLine*, vol. 50, no. 1, pp. 14 680–14 685, 2017.